CrystEngComm

New Germanate and Mixed Cobalt Germanate Salt Inclusion Materials: [(Rb6F)(Rb4F)][Ge14O32] and [(Rb6F)(Rb3.1Co0.9F0.96)][Co3.8Ge10.2O30F2]

Journal:	*CrystEngComm*
Manuscript ID	CE-ART-07-2020-001099.R2
Article Type:	Paper
Date Submitted by the Author:	19-Oct-2020
Complete List of Authors:	Carone, Darren; University of South Carolina, Chemistry and Biochemistry Usman, Mohammad; University of South Carolina, Chemistry and Biochemistry Klepov, Vladislav; University of South Carolina, Department of Chemistry and Biochemistry Smith, Mark; University of South Carolina, Department of Chemistry and Biochemistry Kocevski, Vancho; Los Alamos National Laboratory, Besmann, Theodore; University of South Carolina, Mechanical Engineering Zur Loye, Hans-Conrad; University of South Carolina, Department of Chemistry and Biochemistry

SCHOLARONE™
Manuscripts

New Germanate and Mixed Cobalt Germanate Salt Inclusion Materials: $[(Rb_6F)(Rb_4F)][Ge_{14}O_{32}]$ and $[(Rb_6F)(Rb_{3.1}Co_{0.9}F_{0.96})][Co_{3.8}Ge_{10.2}O_{30}F_2]$

Darren Carone,[1] Mohammad Usman,[1] Vladislav V. Klepov,[1] Mark D. Smith,[1] Vancho Kocevski,[2#] Theodore M. Besmann[2], and Hans-Conrad zur Loye[1]*

[1]*Department of Chemistry and Biochemistry, University of South Carolina, Columbia, SC 29208, USA*
[2]*Nuclear Engineering Program, Department of Mechanical Engineering, University of South Carolina, Columbia, SC 29208, USA*
[#]Current address: MST-8, Los Alamos National Laboratory, Los Alamos, NM 87545, USA.
Email: kocevski@lanl.gov

Abstract

Single crystals of two new germanates, $[(Rb_6F)(Rb_4F)][Ge_{14}O_{32}]$ and $[(Rb_6F)(Rb_{3.1}Co_{0.9}F_{0.96})][Co_{3.8}Ge_{10.2}O_{30}F_2]$, were synthesized via high temperature RbCl/RbF flux growth. Both compounds crystallize in the cubic space group $F\bar{4}3m$ and possess the germanium framework of the previously reported salt inclusion material (SIM), $[(Cs_6F)(Cs_3AgF)][Ge_{14}O_{32}]$, related to the Ge_7O_{16} zeolitic family. These materials demonstrate the ability to accommodate a variety of salt-inclusions, and exhibit chemical flexibility enabling modifications of the framework through incorporation of Co. Alteration of the salt-inclusion led to intrinsic luminescence of $[(Rb_6F)(Rb_4F)][Ge_{14}O_{32}]$ while modification of the framework resulted in an unanticipated Rb/Co salt/inclusion in $[(Rb_6F)(Rb_{3.1}Co_{0.9}F_{0.96})][Co_{3.8}Ge_{10.2}O_{30}F_2]$. Fluorescence measurements were performed on $[(Rb_6F)(Rb_4F)][Ge_{14}O_{32}]$. First-principles calculations in the form of density functional theory (DFT) were performed for $[(Rb_6F)(Rb_{3.1}Co_{0.9}F_{0.96})][Co_{3.8}Ge_{10.2}O_{30}F_2]$ to elucidate its electronic and magnetic properties, and stability at 0 K.

Introduction

Salt inclusion materials, or SIMs, have attracted significant attention as potential nuclear waste forms,[1] and although a significant number of structures and compositions have been reported to date,[2–10] their synthesis/discovery is not readily predictable. Most SIMs have been grown as single crystals out of molten salt fluxes and it has been shown that the salt inclusion typically consists of elements from the molten flux itself. Hence, by choosing different alkali and halide species for the melt that has led to one SIM composition, it is possible to obtain different compositions in a fairly predictable way. Similarly, one can attempt to modify not the salt inclusion, but the framework itself, by adding other framework forming species to the melt. In both cases the energetics i.e., heats of formation, will ultimately determine the ability to create the target phase. While crystals obtained from fluxes need to be relatively thermodynamically stable, they may in fact be metastable structures or compositions whose formation was governed by kinetic and/or steric factors.

Our group recently discovered and structurally characterized a new germanate framework SIM, $[(Cs_6F)(Cs_3AgF)][Ge_{14}O_{32}]$, containing Cs_6F and Cs_3AgF salt inclusion species located in the large channels of the framework.[11] To further investigate this structure type and to explore the extent to which the salt inclusion and/or the framework of the structure could be chemically modified, we explored the synthesis of other germanate SIMs via flux crystal growth. Specifically, we focused on modifying the salt inclusion and on modifying the framework. Interestingly, as discussed within, the salt inclusion could easily be modified and, surprisingly, so could the framework via Co incorporation. The change in the salt inclusion resulted in intrinsic luminescence, while the cobalt incorporation resulted in an unprecedented Rb/Co salt inclusion as well as in the presence of cobalt in the framework itself.

In our previous report,[11] we focused on investigating the promising ion exchange properties of the germanium framework-based salt-inclusion. The Cs structure was found to undergo successful ion exchange with both K and Rb. In the current effort, a family of this structure type is created with the successful synthesis of two new compositions: (1) a Rb salt-inclusion with all germanium framework and (2) a mixed Ge/Co framework with Rb/Co site mixing. The cubic germanate framework has now demonstrated room temperature luminescence in $[(Rb_6F)(Rb_4F)][Ge_{14}O_{32}]$ and the capacity to incorporate 3*d* transition metals in $[(Rb_6F)(Rb_{3.1}Co_{0.9}F_{0.96})][Co_{3.8}Ge_{10.2}O_{30}F_2]$.

Experimental

Reagents

GeO_2 (99.999%, Alfa Aesar), RbCl (Alfa Aesar, 99.8%), and RbF (99.1%, Alfa Aesar) were used as received for the synthesis of both compounds. For the synthesis of $[(Rb_6F)(Rb_{3.1}Co_{0.9}F_{0.96})][Co_{3.8}Ge_{10.2}O_{30}F_2]$, CoF_2 (Alfa Aesar, anhydrous powder, 98%) was used as received.

Synthesis

Single crystals of $[(Rb_6F)(Rb_4F)][Ge_{14}O_{32}]$ were grown out of a eutectic RbCl/RbF flux. To a cylindrical silver crucible welded shut on one end, 2 mmol of GeO_2 were added and covered by 1.70 g of RbCl and 1.30 g of RbF. The silver crucible was crimped shut and placed upright in a programmable box furnace. The reaction mixture was heated at 300 °C/h to 900 °C, held at this temperature for 12 h, slow cooled to 400 °C/h at a rate of 6 °C/h, and then rapidly cooled to room temperature by shutting the furnace off. The solidified flux matrix was dissolved in hot water, aided by sonication, and the products were collected by vacuum filtration and dried with acetone. Colorless, irregular block-shaped crystals approaching 1 mm^3 in size were obtained in approximately 30% yield along with large amounts of AgCl, which was removed from the target phase using a concentrated sodium thiosulfate solution.

For the synthesis of $[(Rb_6F)(Rb_{3.1}Co_{0.9}F_{0.96})][Co_{3.8}Ge_{10.2}O_{30}F_2]$, 1 mmol of CoF_2 and 4 mmol of GeO_2 were layered beneath 3.42 g of RbCl and 2.42 g of RbF in a cylindrical silver crucible. The reaction mixture was heated at 300 °C/h to 850 °C, maintained at this temperature for 24 h, slow cooled to 400 °C at 6 °C/h, and then rapidly cooled to room temperature by shutting the furnace off. Once cooled to ambient temperature, the solidified RbCl/RbF flux was dissolved in distilled water, aided by sonication, and the resulting products were isolated by vacuum filtration. Bright green, irregular block-shaped crystals approximately 0.3 x 0.2 x 0.15 mm^3 in size were obtained in more than 25% yield together with large amounts of powder.

Single-Crystal X-ray Diffraction (SCXRD)

X-ray intensity data from suitable crystals of $[(Rb_6F)(Rb_4F)][Ge_{14}O_{32}]$ and $[(Rb_6F)(Rb_{3.1}Co_{0.9}F_{0.96})][Co_{3.8}Ge_{10.2}O_{30}F_2]$ were collected at 301(2) K using a Bruker D8 QUEST diffractometer equipped with a PHOTON 100 CMOS area detector and an Incoatec microfocus source (Mo Kα radiation, λ = 0.71073 Å) [1]. The raw area detector data frames were reduced and corrected for absorption effects using the SAINT+ and SADABS programs.[12, 13] Initial structural

models were obtained with SHELXT.[14] Subsequent difference Fourier calculations and full-matrix least-squares refinement against F^2 were performed with SHELXL-2018 using the ShelXle interface.[15] The data collection covered 100% of reciprocal space to $2\theta_{max}$ = 66.19 and 75.50º, with an average reflection redundancy of 16.4 and 128.3, for $[(Rb_6F)(Rb_4F)][Ge_{14}O_{32}]$ and $[(Rb_6F)(Rb_{3.1}Co_{0.9}F_{0.96})][Co_{3.8}Ge_{10.2}O_{30}F_2]$, respectively, and R_{int} = 0.047 after absorption correction in both cases.

For both $[(Rb_6F)(Rb_4F)][Ge_{14}O_{32}]$ and $[(Rb_6F)(Rb_{3.1}Co_{0.9}F_{0.96})][Co_{3.8}Ge_{10.2}O_{30}F_2]$ the pattern of systematic absences in the intensity data was consistent with *F*-centering, but showed no screw axes or glide planes. Of the five resulting space group candidates (*F*23, $Fm\bar{3}$, *F*432, *F*-43*m* and $Fm\bar{3}m$), $F\bar{4}3m$ (space group #216) was determined to be the best choice by the development of the structural model described below.

The structure of $[(Rb_6F)(Rb_4F)][Ge_{14}O_{32}]$ was refined to an R_1 value of 3.08 %. Any attempt to account for the trace of Ag that was detected by the elemental analysis (EDS) did not result in any improvement of the model, suggesting that silver particulates from the reaction vessel had adhered to the sample used for EDS analysis, making it appear that silver was present in the sample. Large positive and negative electron density peaks were observed near the Rb2 site, indicating disorder of this site. To account for the disorder, the positive electron density peak was assigned to Rb3 site, and site occupancies were restrained to add up to a single atom. After several refinement cycles, the occupancies of Rb2 and Rb3 refined to 0.28(3) and 0.16(8) and the R_1 value decreased from 3.08 to 1.85%. The Flack parameter after the final refinement cycle was 0.010(18), consistent with the correct absolute structure assignment and the absence of inversion twinning.

The structure of $[(Rb_6F)(Rb_{3.1}Co_{0.9}F_{0.96})][Co_{3.8}Ge_{10.2}O_{30}F_2]$ is extensively disordered, involving split and mixed sites. Accurate determination of composition was limited because of the disorder, and the given compositional uncertainties are likely underestimated. Considerable difficulty was met in achieving a plausible structural model under elemental composition constraints. Semi-quantitative elemental analysis results showed Rb, Ge, Co, O and F as the only significant constituent elements in the crystals, and the structure was modeled using only those elements. Several refinement models were considered, none flawless; the best is presented here. The asymmetric unit in *F*-43*m* consists of one pure Rb site Rb(1A)/Rb(1B), one mixed Rb/Co site Rb(2A)/Co(2A), two mixed Ge/Co sites Ge(1)/Co(1) and Ge(2)/Co(2), one pure Ge site Ge(3), three unique oxygen atoms O(1)-(O3), one mixed O/F site O(4)/F(4) and two pure F sites F(5) and

F(6A)/F(6B). All cation sites have partial or mixed occupancy except for the (pseudo)octahedral germanium site Ge(3) (Wyckoff site 16*e*, .3*m* site symmetry). The Ge(3) site occupation factor (*sof*) refined to 1.003(5) and was fixed at 100% germanium. Sites Ge(1)/Co(1) (24*f*, 2.*mm* site symmetry) and Ge(2)/Co(2) (16*e*, .3*m* symmetry) were initially refined as germanium. The Ge(2) and Ge(3) s*of*s refined to significantly less than 100% Ge Ge(1) = 0.888(6) and Ge(2) = 0.953(5), accompanied by a reduction in the R_1-factor from 0.027 to 0.020. This observation was attributed to mixing of Co(III) onto these sites. A mixed-site Ge/Co model was judged to be more likely than a Ge/vacancy model. The sites were constrained to full occupancy and refined to *sof* Ge(1)/Co(1) = 0.52(3)/0.48(3) and *sof* Ge(2)/Co(2) = 0.78(2)/0.22(2). Site Rb(1) is split over two positions, both on site 24*g* (2.mm symmetry) with refined occupancies Rb(1A) = 0.88(1) and Rb(1B) = 0.10(1). Site Rb(2) was initially refined as pure Rb, but it was necessary to introduce cobalt onto this site cluster to account for a distance of 2.24 Å to the 100%-occupied site O(4)/F(4). This is certainly unreasonably short for a Rb-O/F distance and therefore this site must be occupied by a smaller atom for which Co is the most plausible choice. The Rb part of the site cluster Rb(2A)/Co(2A) is located on site 48*h* (..*m* symmetry), generating three equivalent atoms with occupancies *sof* Rb(2A) = 0.261(5). The Co part is located on site 16*e* (.3*m* symmetry), generating one site with an occupancy of *sof* Co(2A) = 0.224(15). The total Rb(2A)/Co(2A) site cluster occupancy therefore sums to 1.0 within experimental error, providing support for the unusual Co admixture model. Three oxygen atoms O(1) and O(2) on site 48*h*, O(3) on site 16*e* refined to 100% occupied within error. The *sof* for site O(4)/F(4) (site 16*e*) refined to greater than 100% oxygen but less than 100% fluorine and was refined as a 50/50 O/F mixture. Site F(5) (site 4*d*, -43*m* site symmetry) refined to significantly greater than 100% oxygen in trials but refined well as 100% F. The final anion site, F(6), is split over two positions F(6A) on site 4*c* with -43*m* symmetry and F(6B) on site 16*e*. The occupancies of these two sites refined to F(6A) = 0.39(4) and F(6B) = 0.13(2). The above model generates an electroneutral composition of $Rb_{4.51}Ge_{5.10}Co_{2.35}O_{15}F_{1.96}$ (assuming Co^{3+}). All atoms were refined with anisotropic displacement parameters except for minor disorder component atoms Rb(1B), Co(2A) and F(6A)/F(6B). These were refined with a fixed isotropic displacement parameter of 0.025 $Å^2$ for refinement stability. The largest residual electron density peak and hole in the final difference map are +1.45 and -0.72 $e^-/Å^3$, located 1.53 Å from Ge(2)/Co(2) and 0.60 Å from Ge(1)/Co(1), respectively. The Flack after the final refinement cycle was -0.017(8), consistent with the correct absolute structure assignment and the

absence of inversion twinning. Charge balance for the compound may be achieved by assigning +1/+4/+3/-1/-1 to Rb/Ge/Co/O/F. Final unit cell parameters were determined by least-squares refinement of 9092 reflections. Crystallographic and refinement data and selected interatomic distances for both compounds are provided in Tables 1 – 3.

Powder X-ray diffraction (PXRD)

Powder X-ray diffraction data were collected on a Bruker D2 Phaser powder X-ray diffractometer using Cu Kα radiation. The step scan covered the angular range 5-65° 2θ in steps of 0.04°. The experimental and calculated PXRD patterns for $[(Rb_6F)(Rb_4F)][Ge_{14}O_{32}]$ were found to be in good agreement (see Supporting information Fig. S1).

Energy-Dispersive Spectroscopy (EDS)

Elemental analysis was performed on single crystals using a TESCAN Vega-3 SBU SEM with EDS capabilities. The crystals were mounted on carbon tape and analyzed using a 20 kV accelerating voltage and an accumulation time of 1 min. As a qualitative measure, EDS confirmed the presence of Rb, Ge, O, F in $[(Rb_6F)(Rb_4F)][Ge_{14}O_{32}]$ and additionally the presence of Co in $[(Rb_6F)(Rb_{3.1}Co_{0.9}F_{0.96})][Co_{3.8}Ge_{10.2}O_{30}F_2]$. For EDS spectra, see supporting information Figs. S2 and S3.

Fluorescence Spectroscopy

Room temperature emission spectra were collected on a ground sample of $[(Rb_6F)(Rb_4F)][Ge_{14}O_{32}]$ at an excitation wavelength of 258 nm using a Perkin Elmer LS 55 fluorescence spectrometer. For emission measurements the ground sample was placed inside a 6 mm quartz sample holder. Emission scans were performed in the 300 – 800 nm range. Excitation spectra were collected in the 200 – 400 nm range at an emission wavelength of 500 nm.

First-principles Calculations

We performed first-principles calculations for $[(Rb_6F)(Rb_{3.1}Co_{0.9}F_{0.96})][Co_{3.8}Ge_{10.2}O_{30}F_2]$ in the form of density functional theory (DFT) with an on-site Coulomb interaction, i.e., DFT+*U*, using the Vienna Ab-initio Package (VASP) code,[16, 17] using the projector augmented wave (PAW) method[18, 19] and generalized gradient approximation of Perdew, Burke and Ernzerhof (PBE).[20] To model the mixing and partial occupies in the studied compound, we generated super quasi-random structures (SQS) with the experimentally proposed composition $[(Rb_6F)(Rb_{3.1}Co_{0.9}F_{0.96})][Co_{3.8}Ge_{10.2}O_{30}F_2]$, using the mcsqs code provided by the Alloy Theoretic Automated Toolkit (ATAT) toolkit.[21–24] To see if the $[(Rb_6F)(Rb_{3.1}Co_{0.9}F_{0.96})][Co_{3.8}Ge_{10.2}O_{30}F_2]$

system is thermodynamically stable, i.e., it breaks the Rb-Co-Ge-F-O convex hull, we compared its formation energy with respect to Open Quantum Materials Database (OQMD)[25, 26] convex hull. We used the OQMD calculations set-up: 520 eV cut-off energy for the plane wave basis set, 10^{-4} eV energy convergence criterion, 2×2×2 **k**-point mesh for $Rb_{4.51}Co_{2.35}Ge_{5.10}F_{1.96}O_{15}$, and $U_{eff} = 3.3$ eV for the Co atoms. We considered the system to be spin-polarized, with high-spin ferromagnetic (FM) and antiferromagnetic (AFM) (0 μ_B magnetic moment) ordering of the Co atoms.[27] For calculating the electronic and optical properties we performed more rigorous calculations, using 520 eV cut-off energy for the plane wave basis set, 10^{-6} eV and 10^{-3} eV/Å energy and forces convergence criteria, respectively, and the same **k**-point mesh as the OQMD calculations. The ground state geometries were obtained by relaxing the cell volume, cell shape and atomic positions.

Results and Discussion

Synthesis

Crystals of $[(Rb_6F)(Rb_4F)][Ge_{14}O_{32}]$ and $[(Rb_6F)(Rb_{3.1}Co_{0.9}F_{0.96})][Co_{3.8}Ge_{10.2}O_{30}F_2]$ were grown by an enhanced flux growth method using metal halide reagents and reaction vessels that minimized surface area to volume ratios that has been developed to encourage the synthesis of mixed anion compounds as well as other complex germanates, which we previously reported.[2, 3, 28–30] The use of mixed alkali halide fluxes at relatively high temperatures has proven successful for the discovery and crystal growth of numerous new oxyfluoride and salt-inclusion materials.[31–33] The specific conditions used in this work take advantage of the relatively low melting point of the eutectic RbCl/RbF system (540 °C) compared to the synthesis and presumed crystal nucleation temperatures of 850 °C and 900°C for $[(Rb_6F)(Rb_4F)][Ge_{14}O_{32}]$ and $[(Rb_6F)(Rb_{3.1}Co_{0.9}F_{0.96})][Co_{3.8}Ge_{10.2}O_{30}F_2]$, respectively. It is important to notice that the synthesis of $[(Rb_6F)(Rb_{3.1}Co_{0.9}F_{0.96})][Co_{3.8}Ge_{10.2}O_{30}F_2]$ involves CoF_2 as a reagent, instead of a cobalt oxide reagent, which affects the rate of dissolution in the flux.

Crystal Structure

The title compounds are closely related to the previously reported salt inclusion phase $[(Cs_6F)(Cs_3AgF)][Ge_{14}O_{32}]$[11] as all share a large germanium framework and salt-inclusion components within the 3D channels. The nature of the salt inclusion in $[(Rb_6F)(Rb_4F)][Ge_{14}O_{32}]$ and the presence of fluorine in the germanium framework in

$[(Rb_6F)(Rb_{3.1}Co_{0.9}F_{0.96})][Co_{3.8}Ge_{10.2}O_{30}F_2]$, however, differentiate the new compositions from the previously reported $[(Cs_6F)(Cs_3AgF)][Ge_{14}O_{32}]$.

The germanium framework structure of $[(Rb_6F)(Rb_4F)][Ge_{14}O_{32}]$ is derived from GeO_6 octahedra that share edges with one another to form Ge_4O_{16} tetramers. The Ge-O bond lengths for GeO_6 octahedra range from 1.826(3) Å – 1.958(3) Å, in good agreement for what is observed in $[(Cs_6F)(Cs_3AgF)][Ge_{14}O_{32}]$. These tetramers are further connected through edge sharing to intervening GeO_4 tetrahedra to form the overall 3D framework shown in Fig. 1. The Ge-O bond lengths in the GeO_4 tetrahedra range from 1.728(4) Å – 1.749(4) Å consistent with the bond lengths in $[(Cs_6F)(Cs_3AgF)][Ge_{14}O_{32}]$. The framework of $[(Rb_6F)(Rb_4F)][Ge_{14}O_{32}]$ contains large, interconnected channels running down the *a*-, *b*- and *c*-axis in which the salt inclusion is located. The salt inclusion consists of tetrahedral Rb_4F (Rb-F bond lengths of 2.446(16) Å) and octahedral Rb_6F units (Rb-F bond lengths of 2.974(3) Å) that are located in the channels and arranged to occupy alternating channels in an NaCl fashion, shown in Fig. 2. This impacts the size of the unit cell that consists of 8 cubes (2 x 2 x 2). In contrast, the presence of Ag in $[(Cs_6F)(Cs_3AgF)][Ge_{14}O_{32}]$ resulted in the salt inclusions consisting of octahedral Cs_6F and trigonal pyramidal Cs_3AgF units.

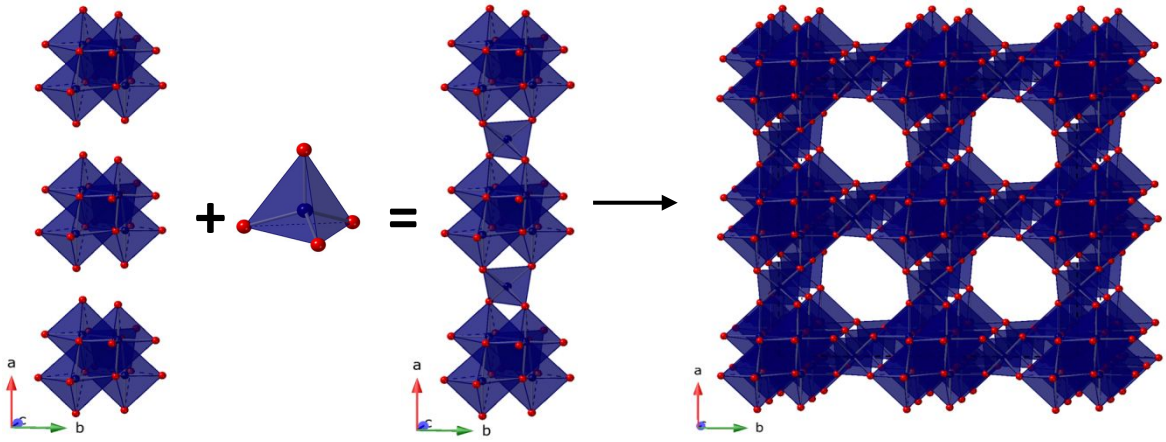

Fig. 1 Germanium oxide framework in $[(Rb_6F)(Rb_4F)][Ge_{14}O_{32}]$ made up of Ge_4O_{16} tetramers and GeO_4 polyhedra. Ge and O are shown in deep blue and red, respectively.

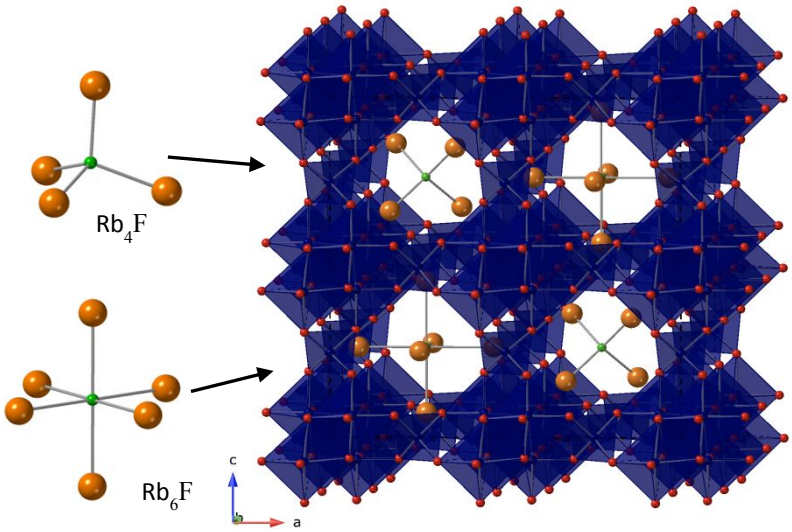

Fig. 2 Structure of $[(Rb_6F)(Rb_4F)][Ge_{14}O_{32}]$ highlighting the arrangement of tetrahedral Rb_4F and octahedral Rb_6F salt inclusions in the channels. Disordered Rb atoms of the Rb_4F tetrahedra are not shown. Rb is shown in orange, F is shown in green, Ge is shown in deep blue, and oxygen is shown in red.

The structure of $[(Rb_6F)(Rb_{3.1}Co_{0.9}F_{0.96})][Co_{3.8}Ge_{10.2}O_{30}F_2]$ is distinct from both $[(Rb_6F)(Rb_4F)][Ge_{14}O_{32}]$ and $[(Cs_6F)(Cs_3AgF)][Ge_{14}O_{32}]$ in that it contains two fluorine atoms in the framework, causing it to be best described as an oxyfluoride framework. The structure is composed of mixed Ge(2)/Co(2)O_6 and Ge(3)$(O/F)_6$ octahedra. The M-O bond lengths for the Ge(2)/Co(2)O_6 octahedra range from 1.839(3) Å – 1.966(2) Å, which is in good agreement with Co-O bond distances taking into account partial site occupation by Ge.[34] The Ge-O bond lengths for the Ge(3)$(O/F)_6$ octahedra range from 1.827(2) Å – 1.9552 (2) Å consistent with the bond lengths for six-coordinated tetravalent Ge.[35] The Ge(2)/Co(2)O_6 octahedra edge-share to form tetramers that are connected in an alternating fashion to Ge(3)$(O/F)_6$ octahedral tetramers via corner-sharing through intervening Ge(1)/Co(1)O_4 tetrahedra in all three dimensions of the crystal structure, creating large channels running down the *a*-, *b*- and *c*-axis. The Co/Ge-O bond lengths in the Ge(1)/Co(1)O_4 tetrahedra range from 1.710(3) Å – 1.724(3) Å. The channels created by the Co/Ge polyhedral network are occupied by fluoride ions, F(5) and disordered F(6), pure rubidium Rb(1) ions and, most strikingly, an unusual mixed Rb(2A)/Co(2A) clusters, shown in Fig. 3. The

arrangement of the Co/Ge- and Ge-based tetramers in the framework columns is reminiscent of the *ABAB* stacking sequence in rock-salt. The complete pictorial representation of the crystal structure assembly for $[(Rb_6F)(Rb_{3.1}Co_{0.9}F_{0.96})][Co_{3.8}Ge_{10.2}O_{30}F_2]$ is provided in Figs. 4 and 5.

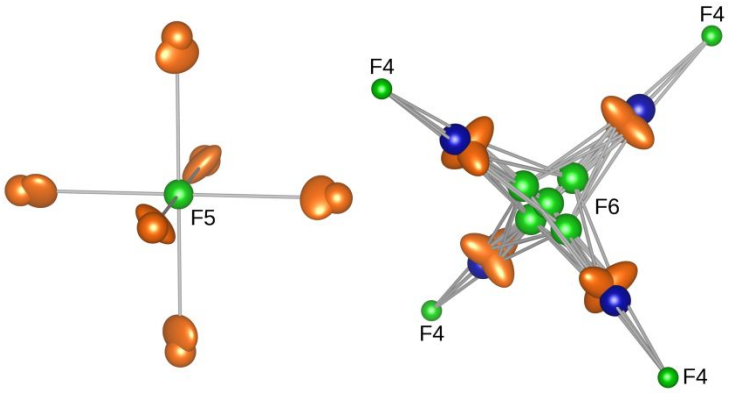

Fig. 3 Representations of the (Rb_6F) octahedral and $(Rb_{3.1}Co_{0.9}F_{0.96})$ tetrahedral salt inclusions in $[(Rb_6F)(Rb_{3.1}Co_{0.9}F_{0.96})][Co_{3.8}Ge_{10.2}O_{30}F_2]$ The F4 anion is part of the framework and directly bonded to Ge. F5 and F6 are part of the salt inclusion. Fluorine atoms are green, rubidium atoms orange and cobalt atoms blue.

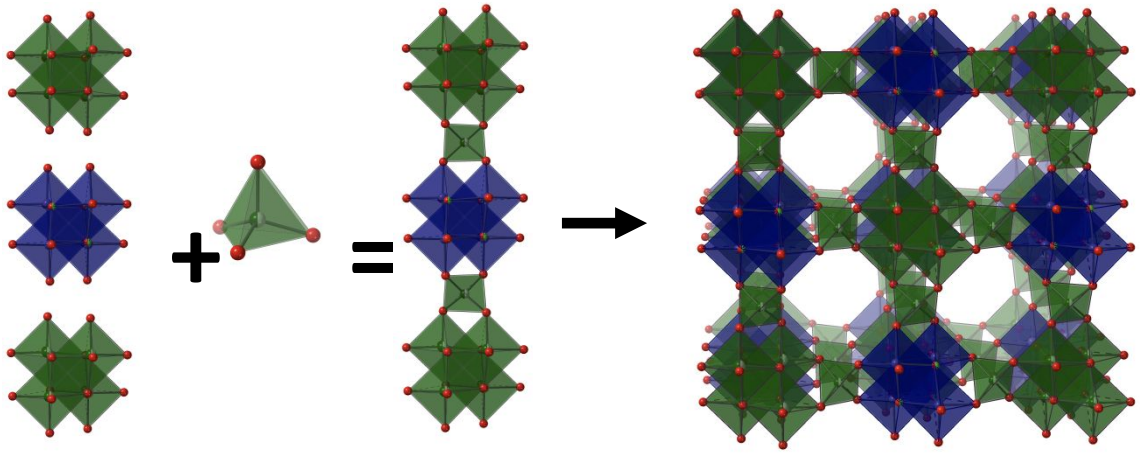

Fig. 4 Assembly of $(Co/Ge)O_6$ and $Ge(O/F)_6$ based tetramers via corner-sharing with $(Co/Ge)O_4$ tetrahedra forming columns that constituent the cobalto-germanate framework in $[(Rb_6F)(Rb_{3.1}Co_{0.9}F_{0.96})][Co_{3.8}Ge_{10.2}O_{30}F_2]$. The mixed Co/Ge and pure Ge octahedra are shown in green and deep blue, respectively. O is shown in red.

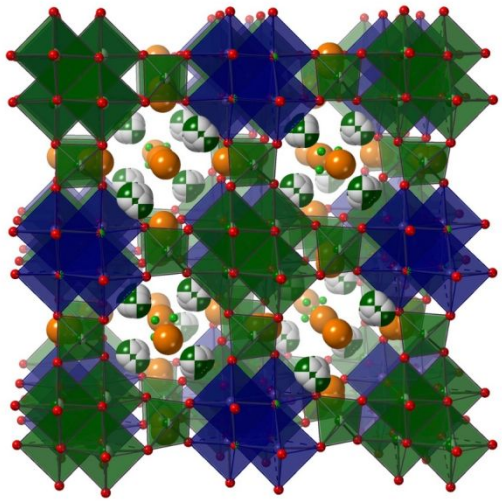

Fig. 5 Projection of the crystal structure of $[(Rb_6F)(Rb_{3.1}Co_{0.9}F_{0.96})][Co_{3.8}Ge_{10.2}O_{30}F_2]$ down the *c*-axis. Pure fluorine and pure rubidium sites are depicted as green and orange spheres, respectively. The mixed green and white spheres represent the mixed Rb/Co clusters in the channels. The mixed Co/Ge and pure Ge octahedra are shown in green and deep blue, respectively. O is shown in red.

Table 1 Crystallographic and refinement data for $[(Rb_6F)(Rb_4F)][Ge_{14}O_{32}]$ and $[(Rb_6F)(Rb_{3.1}Co_{0.9}F_{0.96})][Co_{3.8}Ge_{10.2}O_{30}F_2]$.

Empirical formula	$FGe_7O_{16}Rb_5$	$Co_{2.35}F_{1.96}Ge_{5.10}O_{15}Rb_{4.51}$
Formula weight (g/mol)	1210.53	1171.63
Temperature (K)	301(2)	301(2)
Wavelength (Å)	0.71073	
Crystal system	Cubic	
Space group	*F*-43*m*	
Unit cell dimensions (Å)	a = 15.34580(10)	a = 15.2686(14)
Volume (Å^3) and Z	3613.84(7) and 8	3559.6(10) and 8
Density (calculated) (mg/m^3)	4.450	4.373
Absorption coefficient (mm^{-1})	24.956	22.982
F(000)	4368	4250
Crystal size (mm x mm x mm)	0.04 x 0.04 x 0.04	0.20 x 0.18 x 0.16
Theta range for data collection (°)	2.30 to 33.10	2.310 to 37.752
Index ranges	-23<=h<=19, -23<=k<=21, -23<=l<=17	-26<=h<=26, -26<=k<=26, -26<=l<=26
Reflections collected	12156	69679
Independent reflections	740 [$R_{(int)}$ = 0.0468]	1006 [$R_{(int)}$ = 0.0474]
Data / restraints / parameters	740 / 0 / 46	1006 / 0 / 52
Goodness-of-fit on F^2	1.071	1.127
Final R indices [I>2sigma(I)]	R_1 = 0.0185, wR_2 = 0.0445	R_1 = 0.0200, wR_2 = 0.0514
R indices (all data)	R_1 = 0.0239, wR_2 = 0.0474	R_1 = 0.0238, wR_2 = 0.0530
Largest diff. peak and hole	1.001 and -0.797 e.Å^{-3}	1.454 and -0.718 e.Å^{-3}

Table 2 Select Interatomic Distances (Å) of $[(Rb_6F)(Rb_4F)][Ge_{14}O_{32}]$.

Bond	Distance (Å)
F(5) – Rb(1) x6	2.974(3)
F(2) – Rb(2) x4	2.446(16)
Ge(1) – O(1) x3	1.958(3)
Ge(1) – O(6) x3	1.826(3)
Ge(2) – O(3) x3	1.842(3)
Ge(2) – O(4) x3	1.970(3)
Ge(3) – O(3) x2	1.728(4)
Ge(3) – O(6) x2	1.749(4)

Table 3 Select Interatomic Distances (Å) of $[(Rb_6F)(Rb_{3.1}Co_{0.9}F_{0.96})][Co_{3.8}Ge_{10.2}O_{30}F_2]$. M(1) = Ge(1)/Co(1) = 0.52(3)/0.48(3); M(2) = Ge(2)/Co(2) = 0.78(2)/0.22(2).

Bond	Distance (Å)
M(1) – O(2)	1.710(3)
M(1) – O(2)	1.710(3)
M(1) – O(1)	1.724(3)
M(1) – O(1)	1.724(3)
M(2) – O(2) x3	1.839(3)
M(2) – O(3) x3	1.966(2)
Ge(3) – O(1) x3	1.827(2)
Ge(3) – F(4) x2	1.955(2)
Ge(3) – O(4)	1.955(2)

Photoluminescence

Fig. 6 shows the emission spectrum for $[(Rb_6F)(Rb_4F)][Ge_{14}O_{32}]$, which exhibits considerable luminescence at room temperature. This is in contrast to the previously reported germanium framework SIM, $[(Cs_6F)(Cs_3AgF)][Ge_{14}O_{32}]$, which does not luminesce at room temperature. The emission spectrum of $[(Rb_6F)(Rb_4F)][Ge_{14}O_{32}]$ consists of one broad peak with a maximum at approximately 509 nm, consistent with the yellow-green luminescence color observed in $[(Rb_6F)(Rb_4F)][Ge_{14}O_{32}]$ crystals. The absence of a color center in $[(Rb_6F)(Rb_4F)][Ge_{14}O_{32}]$ and the absence of luminescence in the other members of germanium framework SIMs makes it difficult to make a structural argument for the source of luminescence in this material that appears to be intrinsic to the framework in the case of $[(Rb_6F)(Rb_4F)][Ge_{14}O_{32}]$. One can postulate that the reactive nature of the fluoride salt in the flux, in this case toward the silver reaction vessel, creates defects in the $[(Rb_6F)(Rb_4F)][Ge_{14}O_{32}]$ structure that are too minor or too disordered to be detected by single crystal structure determinations, yet that lead to luminescent behavior.

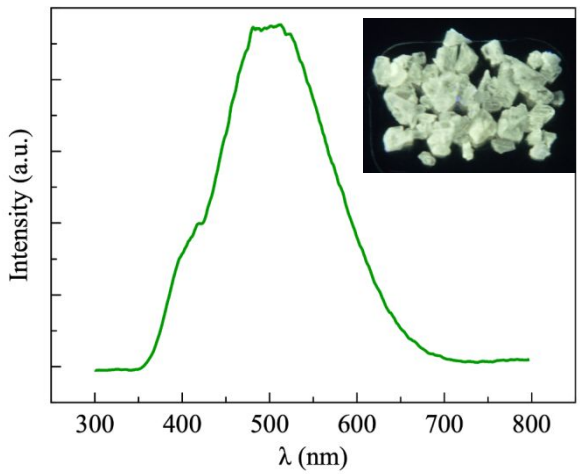

Fig. 6 Emission spectrum at an excitation λ of 258 nm and optical image of $[(Rb_6F)(Rb_4F)][Ge_{14}O_{32}]$ crystals under UV-light.

Attempts were made to tune the luminescence of $[(Rb_6F)(Rb_4F)][Ge_{14}O_{32}]$ by doping it with a small amount of Mn on any of the available Ge sites within the framework. Reactions were

performed as described in the experimental section with the addition of a small percentage of MnO_2. Orange crystals matching the morphology and unit cell of $[(Rb_6F)(Rb_4F)][Ge_{14}O_{32}]$ were prepared, however, the presence of Mn was not detectable in the single crystal X-ray diffraction data and no room temperature luminescence was observed.

Electronic Structure

The DFT calculations for the $[(Rb_6F)(Rb_{3.1}Co_{0.9}F_{0.96})][Co_{3.8}Ge_{10.2}O_{30}F_2]$ structure indicate it relaxes to two ferromagnetic states with high spin (HS) and low spin (LS), having magnetic moments of 3.21 and 0.79 μ_B/Co atom, despite the starting antiferromagnetic configuration of the LS system. The calculated lattice parameters (Table 4) are very close to the experimental values, with an error < 1%. The LS system is more stable, having a 4.8 meV/atom more negative energy compared to the HS system. Both systems do not break the OQMD convex hull with the LS lying 45.8 meV above the convex hull, indicating that these SQS are metastable. Exploring different SQS might yield a slightly more stable state, however, considering that a purely random structure has much higher energy and very different DOS (see supplementary material Figure S4), we believe that a more stable structure would have minuscule effect on DOS and optical properties. The band gaps of the HS system are 1.18 and 1.45 eV in the spin-up and spin-down channel, respectively, while for the LS system are 1.08 and 1.38 eV in the spin up and spin down channel, respectively. From the projected DOS (Figs. 7a and 7b) the HS and LS system the states at the top of the valence band come predominantly from O, while the state at the bottom of the conduction band results from Co, indicating that this compound should behave more like a charge-transfer semiconductor. The different semiconductor character from CoO is caused by the presence of Co-F bonds from the Rb/Co clusters in the framework channels. The bonding with F pushes the Co orbitals to lower energies, decreasing the Co and increasing the O contribution to the states at the top of the valence band. The adsorption indexes of the HS and LS systems are almost identical for energies below 3 eV (Fig. 7d), which arises from the similarity of the HS and LS DOS proximal to their band gaps (Fig. 7c).

Table 4 DFT calculated crystallographic data of $[(Rb_6F)(Rb_{3.1}Co_{0.9}F_{0.96})][Co_{3.8}Ge_{10.2}O_{30}F_2]$. The system relaxed to high spin (HS) and low spin (LS) states.

State	V (Å^3)	a (Å)	b (Å)	c (Å)	β (°)
HS	3539.20	15.2824	15.2824	15.2824	90.0000
LS	3569.97	15.2835	15.2835	15.2835	90.0000

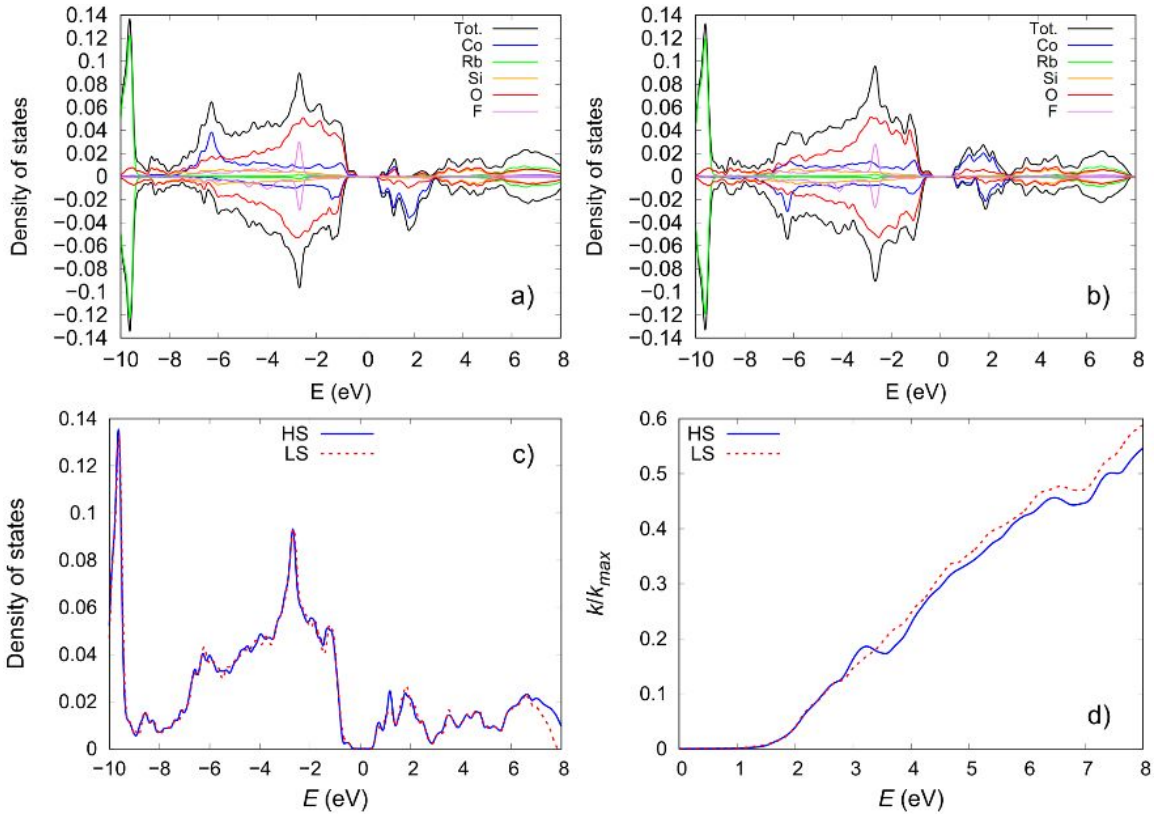

Fig. 7 Projected density of states (PDOS) of $[(Rb_6F)(Rb_{3.1}Co_{0.9}F_{0.96})][Co_{3.8}Ge_{10.2}O_{30}F_2]$ in: a) high spin (HS), and b) low spin (LS) state. The total DOS, Co, Cs, Si and O PDOS are shown in black, blue, green, orange and red, respectively. c) total DOS and d) absorption indexes of $[(Rb_6F)(Rb_{3.1}Co_{0.9}F_{0.96})][Co_{3.8}Ge_{10.2}O_{30}F_2]$ in HS and LS state, shown in blue and red, respectively.

Conclusion

Germanate salt inclusion materials $[(Rb_6F)(Rb_4F)][Ge_{14}O_{32}]$ (**1**) and $[(Rb_6F)(Rb_{3.1}Co_{0.9}F_{0.96})][Co_{3.8}Ge_{10.2}O_{30}F_2]$ (**2**) were synthesized as single crystals using a high temperature RbCl/RbF flux method. Both compounds have the germanate framework observed previously in $[(Cs_6F)(Cs_3AgF)][Ge_{14}O_{32}]$. Modification of the salt inclusion with Rb has led to intrinsic room temperature luminesce of the framework in $[(Rb_6F)(Rb_4F)][Ge_{14}O_{32}]$. Fluorescence measurements show a broad peak with a maximum of approximately 509 nm, consistent with the yellow-green color observed in the crystals under UV light. We have also now demonstrated the ability to incorporate other elements into the framework, in the case of $[(Rb_6F)(Rb_{3.1}Co_{0.9}F_{0.96})][Co_{3.8}Ge_{10.2}O_{30}F_2]$. Incorporation of cobalt resulted in unprecedented Rb/Co mixing within the salt inclusions. First principles calculations for $[(Rb_6F)(Rb_{3.1}Co_{0.9}F_{0.96})][Co_{3.8}Ge_{10.2}O_{30}F_2]$ indicated that its a metastable phase, where the low spin (LS) state is slightly more stable than the high spin (HS) state. The DOS indicate that $[(Rb_6F)(Rb_{3.1}Co_{0.9}F_{0.96})][Co_{3.8}Ge_{10.2}O_{30}F_2]$ has higher charge-transfer semiconductor character, in contrast to CoO, due to the presence of fluorine in the structure.

Acknowledgements

Financial support for this work was provided by the National Science Foundation under DMR-1806279 and is gratefully acknowledged. V. Kocevski and T. M. Besmann acknowledge the use of computational resources provided by the National Energy Research Scientific Computing Center (NERSC) and the HPC cluster Hyperion, supported by The Division of Information Technology at University of South Carolina.

Supplementary information

The crystallographic CIF files for $[(Rb_6F)(Rb_4F)][Ge_{14}O_{32}]$ and $[(Rb_6F)(Rb_{3.1}Co_{0.9}F_{0.96})][Co_{3.8}Ge_{10.2}O_{30}F_2]$ were deposited into the CCDC data base with CCDC numbers of 2014420 and 1905088 (https://www.ccdc.cam.ac.uk).

References

(1) H.-C. zur Loye, T. Besmann, J. Amoroso, K. Brinkman, A. Grandjean, C. H. Henager, S. Hu, S. T. Misture, S. R. Phillpot, N. B. Shustova, H. Wang, R. J. Koch, G. Morrison and E. Dolgopolova, Hierarchical Materials as Tailored Nuclear Waste Forms: A Perspective, *Chem. Mater.,* 2018, **30**, 4475-4488.

(2) G. Morrison, M. D. Smith and H.-C. zur Loye, Understanding the Formation of Salt-Inclusion Phases: An Enhanced Flux Growth Method for the Targeted Synthesis of Salt-Inclusion Cesium Halide Uranyl Silicates, *J. Am. Chem. Soc.,* 2016, **138**, 7121-7129.

(3) G. Morrison and H.-C. zur Loye, Flux Growth of $[NaK_6F][(UO_2)_3(Si_2O_7)_2]$ and $[KK_6Cl][(UO_2)_3(Si_2O_7)_2]$: The Effect of Surface Area to Volume Ratios on Reaction Products, *Cryst. Growth Des.,* 2016, **16**, 1294-1299.

(4) Y.-C. Chang, W.-J. Chang, S. Boudin and K.-H. Lii, High-temperature, high-pressure hydrothermal synthesis and characterization of a salt-inclusion mixed-valence uranium(V,VI) silicate: $[Na_9F_2][(U(V)O_2)(U(VI)O_2)_2(Si_2O_7)_2]$, *Inorg. Chem.,* 2013, **52**, 7230-7235.

(5) C. A. Juillerat, E. E. Moore, G. Morrison, M. D. Smith, T. Besmann and H.-C. zur Loye, Versatile Uranyl Germanate Framework Hosting 12 Different Alkali Halide 1D Salt Inclusions, *Inorg. Chem.,* 2018, **57**, 11606-11615.

(6) C. A. Juillerat, V. V. Klepov, M. D. Smith and H.-C. zur Loye, Targeted crystal growth of uranium gallophosphates via the systematic exploration of the UF_4–$GaPO_4$–ACl (A = Cs, Rb) phase space, *CrystEngComm,* 2020, **22**, 3020-3032.

(7) V. V. Klepov, C. A. Juillerat, E. V. Alekseev and H.-C. zur Loye, Overstepping Löwenstein's Rule-A Route to Unique Aluminophosphate Frameworks with Three-Dimensional Salt-Inclusion and Ion-Exchange Properties, *Inorg. Chem.,* 2019, **58**, 724-736.

(8) C.-S. Lee, S.-L. Wang, Y.-H. Chen and K.-H. Lii, Flux synthesis of salt-inclusion uranyl silicates: $[K_3Cs_4F][(UO_2)_3(Si_2O_7)_2]$ and $[NaRb_6F][(UO_2)_3(Si_2O_7)_2]$, *Inorg. Chem.,* 2009, **48**, 8357-8361.

(9) S. N. Volkov, D. O. Charkin, M. Y. Arsent'ev, A. V. Povolotskiy, S. Y. Stefanovich, V. L. Ugolkov, M. G. Krzhizhanovskaya, V. V. Shilovskikh and R. S. Bubnova, Bridging the Salt-Inclusion and Open-Framework Structures: The Case of Acentric $Ag_4B_4O_7X_2$ (X = Br, I) Borate Halides, *Inorg. Chem.,* 2020, **59**, 2655-2658.

(10) M. J. Winiarski, T. T. Tran, J. R. Chamorro and T. M. McQueen, $(CsX)Cu_5O_2(PO_4)_2$ (X = Cl, Br, I): A Family of Cu^{2+} $S = {}^1/_2$ Compounds with Capped-Kagomé Networks Composed of OCu_4 Units, *Inorg. Chem.,* 2019, **58**, 4328-4336.

(11) N. R. Spagnuolo, G. Morrison and H.-C. zur Loye, Synthesis and crystal structure of $[(Cs_6F)(Cs_3AgF)][Ge_{14}O_{32}]$ through alkali halide flux growth, *Solid State Sci.,* 2019, **97**, 105973.

(12) L. Krause, R. Herbst-Irmer, G. M. Sheldrick and D. Stalke, Comparison of Silver and Molybdenum Microfocus X-Ray sources for Single-Crystal Structure Determination, *J. Appl. Crystallogr.,* 2015, **48**, 3-10.
(13) Bruker, *APEX3*, *SAINT+*, *TWINABS*, and *SADABS*, Bruker AXS Inc., Madison, Wisconsin, USA, 2015.
(14) G. M. Sheldrick, Crystal Structure Refinement with SHELXL, *Acta Crystallogr., Sect. C: Struct. Chem.,* 2015, **71**, 3-8.
(15) C. B. Hübschle, G. M. Sheldrick and B. Dittrich, ShelXle: a Qt graphical user interface for SHELXL., *J. Appl. Crystallogr.,* 2011, **44**, 1281-1284.
(16) G. Kresse and J. Furthmüller, Efficiency of ab-initio total energy calculations for metals and semiconductors using a plane-wave basis set, *Comput. Mater. Sci.,* 1996, **6**, 15-50.
(17) G. Kresse and J. Furthmüller, Efficient iterative schemes for ab initio total-energy calculations using a plane-wave basis set., *Phys. Rev. B,* 1996, **54**, 11169-11186.
(18) P. E. Blöchl, Projector augmented-wave method., *Phys. Rev. B,* 1994, **50**, 17953-17979.
(19) G. Kresse and D. Joubert, From ultrasoft pseudopotentials to the projector augmented-wave method, *Phys. Rev. B,* 1999, **59**, 1758-1775.
(20) J. P. Perdew, K. Burke and M. Ernzerhof, Generalized Gradient Approximation Made Simple, *Phys. Rev. Lett.,* 1996, **77**, 3865-3868.
(21) A. Walle, Multicomponent multisublattice alloys, nonconfigurational entropy and other additions to the Alloy Theoretic Automated Toolkit, *Calphad,* 2009, **33**, 266-278.
(22) A. Walle and G. Ceder, Automating first-principles phase diagram calculations, *J. Phase Equilib,* 2002, **23**, 521-538.
(23) A. Walle, M. Asta and G. Ceder, The Alloy Theoretic Automated Toolkit: A User Guide, *CALPHAD: Comput. Coupling Phase Diagrams Thermochem.,* 2002, **26**, 539-553.
(24) A. Walle and M. Asta, Self-driven lattice-model Monte Carlo simulations of alloy thermodynamic, *Modell. Simul. Mater. Sci. Eng.,* 2002, **10**, 521-538.
(25) S. Kirklin, J. E. Saal, B. Meredig, A. Thompson, J. W. Doak, M. Aykol, S. Rühl and C. Wolverton, The Open Quantum Materials Database (OQMD): assessing the accuracy of DFT formation energies, *npj Comput. Mater.,* 2015, **1**, 15010.
(26) J. E. Saal, S. Kirklin, M. Aykol, B. Meredig and C. Wolverton, Materials Design and Discovery with High-Throughput Density Functional Theory: The Open Quantum Materials Database (OQMD), *JOM,* 2013, **65**, 1501-1509.
(27) Low spin ferromagnetic ordering was also considered, but the calculations always converged to the high spin state.
(28) C. A. Juillerat, V. Kocevski, V. V. Klepov, J. W. Amoroso, T. M. Besmann and H.-C. zur Loye, Structure and Stability of Alkali Gallates Structurally Reminiscent of Hollandite, *J. Am. Ceram. Soc.,* 2020.
(29) M. Usman, M. D. Smith, V. Kocevski, T. Besmann and H.-C. zur Loye, Complex cobalt silicates and germanates crystallizing in a porous three-dimensional framework structure, *CrystEngComm,* 2020, **22**, 1112-1119.

(30) M. Usman, V. Kocevski, M. D. Smith, G. Morrison, W. Zhang, T. Besmann, P. S. Halasyamani and H.-C. zur Loye, Polymorphism and Molten Nitrate Salt-Assisted Single Crystal to Single Crystal Ion Exchange in the Cesium Ferrogermanate Zeotype: $CsFeGeO_4$, *Inorg. Chem.,* 2020.

(31) G. Morrison, T. T. Tran, P. S. Halasyamani and H.-C. zur Loye, $K_8(K_5F)U_6Si_8O_{40}$: An Intergrowth Uranyl Silicate., *Inorg. Chem.,* 2016, **55**, 3215-3217.

(32) C. A. Juillerat, V. Kocevski, G. Morrison, S. G. Karakalos, D. Patil, S. T. Misture, T. M. Besmann and H.-C. zur Loye, Flux crystal growth of uranium(v) containing oxyfluoride perovskites, *Inorg. Chem. Front.,* 2019, **6**, 3203-3214.

(33) G. Morrison, A. M. Latshaw, N. R. Spagnuolo and H.-C. zur Loye, Observation of Intense X-ray Scintillation in a Family of Mixed Anion Silicates, $Cs_3RESi_4O_{10}F_2$ (RE = Y, Eu-Lu), Obtained via an Enhanced Flux Crystal Growth Technique, *J. Am. Chem. Soc.,* 2017, **139**, 14743-14748.

(34) A. M. T. Bell and C. M. B. Henderson, Rietveld Refinement of the Orthorhombic *Pbca* Structures of $Rb_2CdSi_5O_{12}$, $Cs_2MnSi_5O_{12}$, $Cs_2CoSi_5O_{12}$, and $Cs_2NiSi_5O_{12}$ Leucites by Synchrotron X-ray Powder Diffraction, *Acta Cryst.,* 1996, **C52**, 2132-2139.

(35) A. L. Hector, A. Jolleys, W. Levason, D. Pugh and G. Reid, The preparation and structure of Ge_3F_8 - a new mixed-valence fluoride of germanium, a convenient source of GeF_2, *Dalton Trans.,* 2014, **43**, 14514-14516.

TOC for New Germanate and Mixed Cobalt Germanate Salt Inclusion Materials: $[(Rb_6F)(Rb_4F)][Ge_{14}O_{32}]$ and $[(Rb_6F)(Rb_{3.1}Co_{0.9}F_{0.96})][Co_{3.8}Ge_{10.2}O_{30}F_2]$

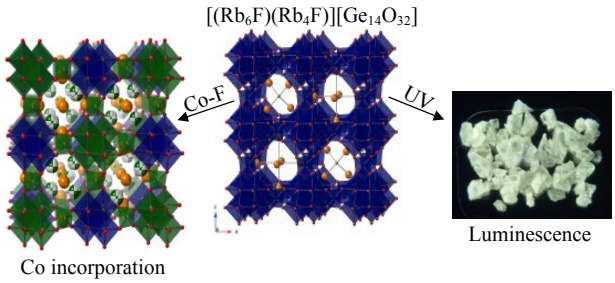

New germanate salt inclusion materials $[(Rb_6F)(Rb_4F)][Ge_{14}O_{32}]$ **(1)** and $[(Rb_6F)(Rb_{3.1}Co_{0.9}F_{0.96})][Co_{3.8}Ge_{10.2}O_{30}F_2]$ **(2)** were grown as single crystals. **(1)** exhibits room temperature luminescence and **(2)** demonstrates Co/Ge mixing in the framework and contains an unanticipated Rb/Co inclusion.